J Math Imaging Vis 26: 115–125, 2006

DOI: 10.1007/s10851-006-8303-2

A New Diffusion-Based Variational Model for Image Denoising and Segmentation

FANG LI
Department of Mathematics, East China Normal University, Shanghai 200062, China Department of Mathematics, South West University, Chongqing 400715, China
lifangswnu@126.com

CHAOMIN SHEN
Joint Laboratory for Imaging Science & Technology, and Department of Computer Science, East China Normal University, Shanghai 200062, China
cmshen@cs.ecnu.edu.cn

LING PI
Department of Applied Mathematics, Shanghai Jiaotong University, Shanghai 200030, China
plingzh@eyou.com

Published online: 25 September 2006

Abstract. In this paper we propose a new variational model for image denoising and segmentation of both gray and color images. This method is inspired by the complex Ginzburg–Landau model and the weighted bounded variation model. Compared with active contour methods, our new algorithm can detect non-closed edges as well as quadruple junctions, and the initialization is completely automatic. The existence of the minimizer for our energy functional is proved. Numerical results show the effectiveness of our proposed model in image denoising and segmentation.

Keywords: image denoising, segmentation, bounded variation function, Ginzburg-Landau model, heat flow

1. Introduction

Image denoising and segmentation are fundamental problems in both image processing and computer vision with numerous applications. The aim of image denoising is to smooth a noisy image without losing significant features, while the aim of image segmentation is to divide an image into several meaningful regions such that each region is relatively homogeneous. These two problems are always correlated.

Variational methods have been extensively studied in image denoising and segmentation because of their flexibility in modeling and various advantages in the numerical implementation. The basic idea of variational methods is to minimize an energy functional. This functional generally will depend on the features of the image. The classical way to solve the minimization problem is to solve the corresponding Euler-Lagrange equation or its associated flow.

The active contour/snake model is one of the most well known variational models for image segmentation [6, 10, 13]. However, this model has one major disadvantage: the result is heavily influenced by the choice of initial contour. Given an initial curve, during the evolution, the energy may evolve to its global or local minimum. Only the curve corresponding to global minimum is the real boundary of the object(s). Thus, the choice of initial curve is very crucial. Moreover,

in numerical experiments, the level set method is usually used, but this method is computationally expensive since it works in higher dimension space than the image space itself.

Another variational method for image denoising and segmentation is based on diffusion. Chen and Wunderli [12] proposed a weighted Bounded Variation (BV) model for gray image restoration by minimizing the following energy functional

$$E(u) = \int_\Omega g(x)|\nabla u| + \frac{\beta}{2}\int_\Omega (u-f)^2\,dx,$$

where f is the observed gray image, $g(x)$ is the diffusion coefficient, and β is a positive parameter.

There are many approaches for color image denoising or segmentation [5, 7, 9, 17–19]. We shall use the Red-Green-Blue (RGB) model of color images here. In what follows, for each pixel $p = (x_1, x_2)$, the vector-valued $u(p) = (u^1(p), u^2(p), u^3(p))$ represents the intensity of the three primary colors separately. Each monochromatic component u^i $(i = 1, 2, 3)$ is one channel.

In this paper we shall propose a new variational model for image denoising and segmentation of both gray and color images. This model is inspired by the complex Ginzburg–Landau (GL) model and the weighted bounded variation model. The remainder of the paper is organized as follows: In Section 2, we give some preliminaries and definitions of vector-valued BV functions. In Sections 3 and 4, the new model for gray and color images are proposed respectively. Theoretical results, iterating scheme and experimental results are given in both sections. Finally, we conclude our paper in Section 5.

2. Preliminaries and Definitions of Vector-Valued BV Functions

Many image processing methods are based on a minimization of functional involving the bounded variation norm [2–3, 8, 12, 15, 16, 20]. The space of functions with bounded variation is called BV space. It is widely accepted that the BV space is a good model for image processing since the real images may have jumps. The BV model performs better than the corresponding Sobolev models in the aspects of keeping important information such as edges. For instance, image denoising can be efficiently done by minimizing the Rudin-Osher-Fatemi (ROF) functional in the category of BV space [16]. Sometimes, substituting BV space by weighted BV space will give even better results in image denoising and segmentation [3, 12].

In this paper, we discuss not only gray images but also color images. Therefore, it is crucial to generalize the definition and basic properties of BV space to vector-valued functions. In what follows, let Ω be a bounded open subset of R^n, and $u : \Omega \to R^m$ be a vector-valued function. Denote the vector-valued Sobolev space $W^{1,1}(\Omega, R^m)$ by $W^{1,1}(\Omega)$, $L^1(\Omega, R^m)$ by $L^1(\Omega)$, etc.

Definition 2.1. (*BV for vector-valued functions*). Assume $u \in L^1(\Omega)$ and the components of u are denoted by $u^\alpha (\alpha = 1, \ldots, m)$. Then we define $u \in BV(\Omega, R^m)$ (BV for short), if u satisfies

$$\begin{aligned}|u|_{BV} &= \sup_\phi \left\{ \int_\Omega u\,\mathrm{div}(\phi)\,dx \,|\, \phi = (\phi^1, \ldots, \phi^m),\right.\\ &\qquad \left. \phi^\alpha \in C_0^1(\Omega, R^n), \alpha = 1, \ldots, m, |\phi(x)| \le 1 \right\}\\ &= \sup_\phi \left\{ \int_\Omega \sum_{\alpha=1}^m u^\alpha \,\mathrm{div}(\phi^\alpha)\,dx \,|\, \phi^\alpha \right.\\ &\qquad \left. \in C_0^1(\Omega, R^n), |\phi(x)| \le 1 \right\} < \infty,\end{aligned}$$

where $\phi^\alpha = (\phi_1^\alpha, \ldots, \phi_n^\alpha)$ and $|\phi(x)| = \sqrt{\sum_{\alpha=1}^m \sum_{i=1}^n (\phi_i^\alpha)^2}$. With the norm

$$\|u\|_{BV} = |u|_{BV} + \|u\|_{L^1(\Omega)}$$

the space of all functions $u \in BV$ becomes a Banach space. If $u \in BV$, $|u|_{BV}$ is called the BV semi-norm of u, and $\|u\|_{BV}$ is called the BV norm of u.

If $u \in W^{1,1}(\Omega)$, we have

$$\begin{aligned}&\sup_{|\phi|\le 1} \int_\Omega \sum_{\alpha=1}^m u^\alpha \,\mathrm{div}(\phi^\alpha)\,dx\\ &\quad = \sup_{|\phi|\le 1} \int_\Omega \sum_{\alpha=1}^m \sum_{i=1}^n u^\alpha\,(\phi_i^\alpha)_i\,dx\\ &\quad = \sup_{|\phi|\le 1} \int_\Omega \left(-\sum_{\alpha=1}^m \sum_{i=1}^n u_i^\alpha \right) \phi_i^\alpha\,dx\\ &\quad = \sup_{|\phi|\le 1} \int_\Omega \nabla u \cdot \phi\,dx,\end{aligned}$$

where $\nabla u = (\nabla u^1, \ldots, \nabla u^m)$, $\phi = (\phi^1, \ldots, \phi^m)$. Since the supremum in the last equality can be attained by $\phi = \frac{\nabla u}{|\nabla u|}$, we have

$$|u|_{BV} = \int_\Omega \nabla u \cdot \frac{\nabla u}{|\nabla u|}\,dx = \|\nabla u\|_{L^1(\Omega)}.$$

That is to say, if $u \in W^{1,1}(\Omega)$, then $\|u\|_{W^{1,1}(\Omega)} = \|u\|_{BV}$.

Theorem 2.2 (lower semicontinuity). *Let $\{u_k\} \subset L^1(\Omega)$ be a sequence of BV functions and $u \in BV$, if $u_k \to u$ strongly in $L^1(\Omega)$, then*

$$|u|_{BV} \le \liminf_{k\to\infty} |u_k|_{BV}.$$

Proof: For fixed $\phi = (\phi^1, \ldots, \phi^m)$, $\phi^\alpha \in C_0^1(\Omega, R^n)$, $\alpha = 1, \ldots, m$, $|\phi(x)| \le 1$, we have

$$\begin{aligned}
&\int_\Omega \sum_{\alpha=1}^m u^\alpha \operatorname{div}(\phi^\alpha)\, dx \\
&\quad = \lim_{k\to\infty} \int_\Omega \sum_{\alpha=1}^m u_k^\alpha \operatorname{div}(\phi^\alpha)\, dx \\
&\quad \le \liminf_{k\to\infty} \sup_{\phi^\alpha} \int_\Omega \sum_{\alpha=1}^m u_k^\alpha \operatorname{div}(\phi^\alpha)\, dx \\
&\quad = \liminf_{k\to\infty} |u_k|_{BV}.
\end{aligned}$$

Taking supremum over $\{\phi = (\phi^1, \ldots, \phi^m) | \phi^\alpha \in C_0^1(\Omega, R^n), \alpha = 1, \ldots, m\}$, we conclude that

$$|u|_{BV} \le \liminf_{k\to\infty} |u_k|_{BV}.$$

□

Theorem 2.3 (compactness). *Let $\{u_k\}$ be a bounded vector-valued sequence in BV space. Assume that $\Omega \subset R^n$ is such that $\partial\Omega$ is Lipschitz. Then there is a subsequence of $\{u_k\}$, also denoted by $\{u_k\}$, and a $u \in BV$ such that $u_k \to u$ strongly in $L^1(\Omega)$.*

Proof: Similar to [14], we can prove the compactness theorem for vector-valued BV space. □

In our model, the weighted BV norm for vector-valued image will be used. The definition of weighted BV functions is given as follows.

Definition 2.4 (weighted BV functions). Assume $u \in L^1(\Omega)$, and $g(x)$ is a nonnegative function. We define $u \in g - BV$, if u satisfies

$$\begin{aligned}
&|u|_{g-BV} \\
&\quad = \sup \left\{ \int_\Omega \sum_{\alpha=1}^m u^\alpha \operatorname{div}(\phi^\alpha)\, dx | \phi^\alpha \in C_0^1(\Omega, R^n), \right. \\
&\qquad \left. \alpha = 1, \ldots, m, |\phi(x)| \le g \right\} < \infty.
\end{aligned}$$

If $u \in g - BV$, $|u|_{g-BV}$ is called the $g - BV$ semi-norm of u.

The lower semicontinuity for $g - BV$ functions can be proved using the similar method in Theorem 2.2.

3. The Proposed Model for Gray Images

The GL model has shown its efficiency for modeling many phenomena in physics, especially in the theory of superconductors [1, 4, 11]. The GL functional is defined as follows,

$$E_\varepsilon(u) = \frac{1}{2} \int_\Omega \left(|\nabla u|^2 + \frac{1}{2\varepsilon^2}(1 - |u|^2)^2 \right) dx, \quad (1)$$

where ε is a small dimensionless constant called the coherence length which depends only on the material and the temperature, u is a complex-valued function indicating the local state of the material: if $|u| \approx 1$ the material is in a superconducting phase, while if $|u| \approx 0$ it is in its normal phase (with no superconducting property). The normal phase is localized in small regions called vortices surrounded by superconducting regions [1]. Our algorithm is inspired by the property that the GL model is able to detect the normal phase. Thus, normal and superconducting phases can be distinguished. In our new model, we expect that the edges correspond to normal phase and other regions correspond to superconducting phase. Hence edges could be detected.

Now assume $f : \Omega \subset R^2 \to R$ be the observed gray image. We should first convert the image $f(x)$ into a complex-valued function u_0. The initialization procedure is as follows. To construct u_0, first we rescale $f(x)$ to the interval $[-1, 1]$ by the formula $v_0 = \frac{2f(x)}{255} - 1$, and assume $w_0 = \sqrt{1 - v_0^2}$, then we define $\operatorname{Re}(u_0) = v_0$ and $\operatorname{Im}(u_0) = w_0$ so that $|u_0| = 1$. Compared with the construction of initial level set function (where signed distance function is usually used) in the active contour method, our initialization is easier and automatic.

Inspired by the complex GL model and weighted BV model, we now construct our model by modifying (1). Firstly, we modify the first term. As analyzed in Section 2, we will use vector-valued $g - BV$ semi-norm to substitute the Sobolev norm in GL model. Secondly, we retain the second term since our new model is expected to have the similar ability to detect the edges as the normal phase in GL model. In our case, the counterpart of normal phase is the edges. Finally, in order to keep the important information in the initial image, we add a fidelity term $\int_\Omega |u - u_0|^2 dx$ in our model. Hence, our

proposed model is to minimize the following energy in $g - BV \cap L^4(\Omega)$.

$$\begin{aligned} F_\varepsilon(u) : &= \mu \sup_{|\phi(x)|\le g} \int_\Omega u \,\mathrm{div}(\phi)\, dx \\ &\quad + \frac{1}{4\varepsilon^2}\int_\Omega (1-|u|^2)^2 dx \\ &\quad + \frac{\lambda}{2}\int_\Omega |u-u_0|^2 dx \\ &= \mu\,|u|_{g-BV} \\ &\quad + \frac{1}{4\varepsilon^2}\int_\Omega (1-|u|^2)^2\, dx \\ &\quad + \frac{\lambda}{2}\int_\Omega |u-u_0|^2\, dx\,, \end{aligned} \tag{2}$$

where $g(x)$ is a diffusion coefficient. In order to preserve edges, our diffusion coefficient is set as

$$g(x) = \frac{1}{1+|\nabla(G_\sigma * f)|^2/k^2} = \frac{1}{1+|\nabla G_\sigma * f|^2/k^2}, \tag{3}$$

where G_σ is the Gaussian kernel with standard deviation σ, and the parameter k models the size of discontinuity. The lager the noise is, the larger we set σ.

In the following, we shall explain further why the proposed energy functional is defined as (2).

(I) In the first term of (2), $g(x)$ serves the purpose of selecting which locations to be smoothed. In regions with small gradient, $g(x)$ is big so that these regions are smoothed. At the locations with large gradient, $g(x)$ is small so that these regions are less smoothed. Then noise can be erased from the noisy images while sharp edges are kept.

Because of the use of *g-BV* semi-norm in the first term, our model performs better in denoising and segmentation than [1] where Sobolev norm $\mu\int_\Omega g\,|\nabla u|^2 dx$ is used.

(II) From the second term, it can be derived that $|u| \approx 1$ almost everywhere after enough diffusion except for the points along the edges of objects, i.e., $|u| \approx 1$ in smooth regions, and $|u|$ is near zero along edges.

(III) The third term is a fidelity term which forces u to be a close approximation of the original image u_0.

Let u be a minimizer of $F_\varepsilon(u)$, then u satisfies the Euler-Lagrange equation

$$\begin{aligned} -\mu\cdot\mathrm{div}\left(g(x)\frac{\nabla u}{|\nabla u|}\right) - \frac{1}{\varepsilon^2}u\,(1-|u|^2) \\ +\lambda\,(u-u_0) = 0 \end{aligned} \tag{4}$$

in Ω and we assume the Neumann boundary condition $\frac{\partial u}{\partial n} = 0$ on $\partial\Omega$ (where n is the outward unit normal to $\partial\Omega$).

In order to solve (4), we use the steepest descent method. Let $u = (v, w)$, then we get the following heat flows with respect to the real and imaginary part of complex-valued image u:

$$\begin{aligned} \frac{\partial v}{\partial t} &= \mu\cdot\mathrm{div}\left(g(x)\frac{\nabla v}{\sqrt{|\nabla v|^2+|\nabla w|^2}}\right) \\ &\quad + \frac{1}{\varepsilon^2}v\,(1-(v^2+w^2)) - \lambda\,(v-v_0), \end{aligned} \tag{5}$$

$$\begin{aligned} \frac{\partial w}{\partial t} &= \mu\cdot\mathrm{div}\left(g(x)\frac{\nabla w}{\sqrt{|\nabla v|^2+|\nabla w|^2}}\right) \\ &\quad + \frac{1}{\varepsilon^2}w\,(1-(v^2+w^2)) - \lambda\,(w-w_0). \end{aligned} \tag{6}$$

with initial value $u_0 = (v_0, w_0)$ and Neumann boundary condition $\frac{\partial u}{\partial n} = 0$ on $\partial\Omega$.

3.1. Mathematical Results

Theorem 3.1 (existence of the minimizer)**.** *There exists a complex-valued function $u_* \in g - BV \cap L^4(\Omega)$ minimizing F_ε, where ε is a fixed positive constant.*

Proof: Rewrite the energy (2) as

$$\begin{aligned} F_\varepsilon(u) = \mu\,|u|_{g\text{-}BV} + \frac{1}{4\varepsilon^2}\int_\Omega (1-|u|^2)^2\, dx \\ + \frac{\lambda}{2}\int_\Omega |u-u_0|^2\, dx. \end{aligned}$$

Since zero is the lower bound of F_ε, we can assume $0 \le \beta = \inf_{u\in V} F_\varepsilon$ and let $\{u_n\}$ be a complex–valued minimizing sequence in $g - BV \cap L^4(\Omega)$, i.e., $\lim_{n\to\infty} F_\varepsilon(u_n) = \beta$. Hence there is a constant $M > 0$ such that

$$\begin{aligned} F_\varepsilon(u_n) = \mu\,|u_n|_{g\text{-}BV} + \frac{1}{4\varepsilon^2}\int_\Omega (1-|u_n|^2)^2\, dx \\ + \frac{\lambda}{2}\int_\Omega |u_n-u_0|^2\, dx < M. \end{aligned} \tag{7}$$

Since $f \in L^\infty(\Omega)$ (in fact,$|f| \le 255$), according to (3) we have $g \ge 1/(1 + C\,\|f\|^2_{L^\infty(\Omega)})$, where $C > 0$ is a constant. So we choose $\delta = 1/(1+ C\,\|f\|^2_{L^\infty(\Omega)})$. Since $g \ge \delta$, we have

$$\mu\,\delta\,|u_n|_{BV} \le \mu\,|u_n|_{g-BV} < M.$$

So $|u_n|_{BV}$ is bounded. The formula (7) also implies that $\{u_n\}$ is bounded in both $L^4(\Omega)$ and $L^2(\Omega)$. Since the imbedding $L^2(\Omega) \to L^1(\Omega)$ is continuous, $\{u_n\}$ is bounded in $L^1(\Omega)$. Then by Definition 2.1, $\{u_n\}$ has bounded BV norm. Therefore Theorem 2.3 shows that there is a subsequence, also denoted by $\{u_n\}$, and $u_* \in BV(\Omega)$ such that $u_n \to u_*$ strongly in $L^1(\Omega)$. Furthermore, by the lower semicontinuity for $g - BV$ space we get

$$|u_*|_{g-BV} \le \liminf_{k\to\infty} |u_n|_{g-BV}\,. \tag{8}$$

(8) also implies $u_* \in g - BV$.

On the other hand, from the boundedness of $\{u_n\}$ in $L^4(\Omega)$, there is a subsequence, also denoted by $\{u_n\}$, converges weakly to u_* by the uniqueness of limit. Hence, $u_* \in L^4(\Omega)$. By the lower semi-continuity of L^2 and L^4 norm, we obtain

$$\int_\Omega (1 - |u_*|^2)^2\,dx \le \liminf_{n\to\infty} \int_\Omega (1 - |u_n|^2)^2\,dx, \tag{9}$$

$$\int_\Omega |u_* - u_0|^2\,dx \le \liminf_{n\to\infty} \int_\Omega |u_n - u_0|^2\,dx. \tag{10}$$

Formulas (8–10) imply the weak lower semicontinuity of F_ε

$$F_\varepsilon(u_*) \le \liminf_{n\to\infty} F_\varepsilon(u_n) = \beta.$$

Therefore, the infimum is attained by $u_* \in g - BV \cap L^4(\Omega)$ and it is a minimizer of the energy F_ε. □

3.2. Numerical Implementation of the Model

We use finite difference scheme to discretize Eqs. (5) and (6). Denote the space step by $h = 1$ and the time step by τ, we have

$$\begin{aligned}
\left(D_x^{\pm} u\right)_{i,j} &= \pm\,[u_{i\pm1,j} - u_{i,j}],\\
\left(D_y^{\pm} u\right)_{i,j} &= \pm\,[u_{i,j\pm1} - u_{i,j}],\\
|(D\,u)_{i,j}| &= \sqrt{((D_x^+ u)_{i,j})^2 + ((D_y^+ u)_{i,j})^2 + \gamma},
\end{aligned}$$

where γ is a small number used to avoid division by zero. To simplify the notations, we will omit the subscripts i, j and use v^k, w^k to denote $v^k_{i,j}$, $w^k_{i,j}$. The iteration formulas are given by

$$\begin{aligned}
v^{k+1} &= v^k + \tau\Big(A^k + \frac{1}{\varepsilon^2} v^k(1 - (v^k)^2 - (w^k)^2)\\
&\qquad - \lambda\,(v^k - v_0)\Big),\\
w^{k+1} &= w^k + \tau\Big(B^k + \frac{1}{\varepsilon^2} w^k(1 - (v^{k+1})^2 - (w^k)^2)\\
&\qquad - \lambda\,(w^k - w_0)\Big),
\end{aligned}$$

where

$$\begin{aligned}
A^k &= \mu \cdot \left(D_x^-\left(g\frac{D_x^+ v^k}{\sqrt{|D\,v^k|^2 + |D\,w^k|^2}}\right)\right.\\
&\qquad \left. + D_y^-\left(g\frac{D_y^+ v^k}{\sqrt{|D\,v^k|^2 + |D\,w^k|^2}}\right)\right),\\
B^k &= \mu \cdot \left(D_x^-\left(g\frac{D_x^+ w^k}{\sqrt{|D\,v^k|^2 + |D\,w^k|^2}}\right)\right.\\
&\qquad \left. + D_y^-\left(g\frac{D_y^+ w^k}{\sqrt{|D\,v^k|^2 + |D\,w^k|^2}}\right)\right).
\end{aligned}$$

3.3. Experimental Results

The proposed variational method has been applied to a variety of synthetic and real gray images. We choose the parameters as $\varepsilon = 1$, $\lambda = 0.01$, $\tau = 0.1$, and μ is a constant between 0.1 and 5, which should be tuned from case to case in every image.

In our experiments for gray images, we get v and w after evolution. The segmented image is displayed by $255\cdot(v^2+w^2)^{100}$ and the denoised image is displayed by $(v+1)\cdot 255/2$. The reason for using $255\cdot(v^2+w^2)^{100}$ is as follows: as seen from (II) in the beginning of Section 3, by the second term in (2), u has the following property after enough diffusion: $|u| \approx 1$ in the smoothed regions, and $|u|$ is near zero along edges. i.e.,

$$(v^2 + w^2)^{100} \approx \begin{cases} 1 & \text{smoothed regions}\\ 0 & \text{along edges} \end{cases}$$

Thus,

$$255 \cdot (v^2 + w^2)^{100} \approx \begin{cases} 255 & \text{smoothed regions}\\ 0 & \text{along edges} \end{cases}$$

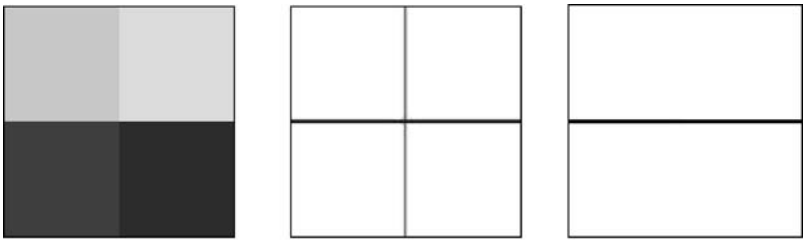

Figure 1. An example of segmentation of a simple image. (a) Original image. (b) Result of segmentation using our model. (c) Result of segmentation using method proposed in [1]. ($\mu = 0.1$, $\tau = 0.1$, $\sigma = 0.1$, $k = 0.5$, iteration $= 5$).

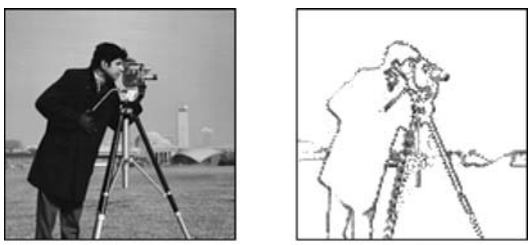

Figure 2. An example of segmentation of the image of camera man. (a) Original image. (b) Result of segmentation. ($\mu = 0.1$, $\tau = 0.1$, $\sigma = 0.1$, $k = 0.1$, iteration $= 100$).

Therefore, as a result of segmentation, the edges are displayed in dark while the smoothed regions are in bright. The reason for using $(v + 1) \cdot 255/2$ as the denoised image is that $(v + 1) \cdot 255/2$ is the rescaling of v, which is smoothed from the rescaled initial image v_0 by the evolution Eqs. (5) and (6).

In Fig. 1, the four regions of constant intensity (see Fig. 1(a)) are segmented by two lines (see Fig. 1(b)). Our proposed model can detect non-closed curves and quadruple junctions. This result is hard to achieve by using active contour method or the diffusion model in [1] by which only the horizontal line can be detected (see Fig. 1(c)). Our model successfully segments the image of camera man in Fig. 2 and the MRI image of head in Fig. 3. In Fig. 4, gaussian noise with signal-to-noise-ratio (SNR) 8.4 is added to Fig. 4(a). Our model yields good results for denoising and segmentation.

4. The Proposed Model for Color Images

Our method can also be adapted to color images. The similar energy is used as before, but now the image u is regarded as a real vector-valued function, i.e., $u : \Omega \subset R^2 \to R^3$, where $u = (u_1, u_2, u_3)$.

The energy functional is written as:

$$F_\varepsilon(u) = \mu\,|u|_{g-BV} + \frac{1}{4\varepsilon^2}\int_\Omega ((1-|u_1|^2)^2 + (1-|u_2|^2)^2 + (1-|u_3|^2)^2)dx + \frac{\lambda}{2}\int_\Omega |u-u_0|^2 dx, \tag{11}$$

where $u_0 = (u_{01}, u_{02}, u_{03}) : \Omega \subset R^2 \to R^3$ is obtained by rescaling the observed RGB image $f : \Omega \subset R^2 \to R^3$ to the cube$[-1, 1] \times [-1, 1] \times [-1, 1]$ with the formula $u_0 = \frac{2f}{255} - (1, 1, 1)$. The diffusion coefficient $g(x)$ is

$$g(x) = \frac{1}{1 + |\nabla G_\sigma * f|^2/k^2}. \tag{12}$$

As before, we get the following heat flow for energy (11) using the steepest descent method.

$$\frac{\partial u_i}{\partial t} = \mu \cdot \operatorname{div}\left(g(x)\frac{\nabla u_i}{\sqrt{|\nabla u_1|^2 + |\nabla u_2|^2 + |\nabla u_3|^2}}\right) + \frac{1}{\varepsilon^2}u_i\,(1-|u_i|^2) - \lambda\,(u_i - u_{0i}), \quad i=1,\ldots,3, \tag{13}$$

in Ω, with initial condition $u|_{t=0} = u_0$ and Neumann boundary condition $\frac{\partial u}{\partial n} = 0$ on $\partial\Omega$.

4.1. Mathematical Results

Using the same techniques as in Section 3, with small modification, we can prove

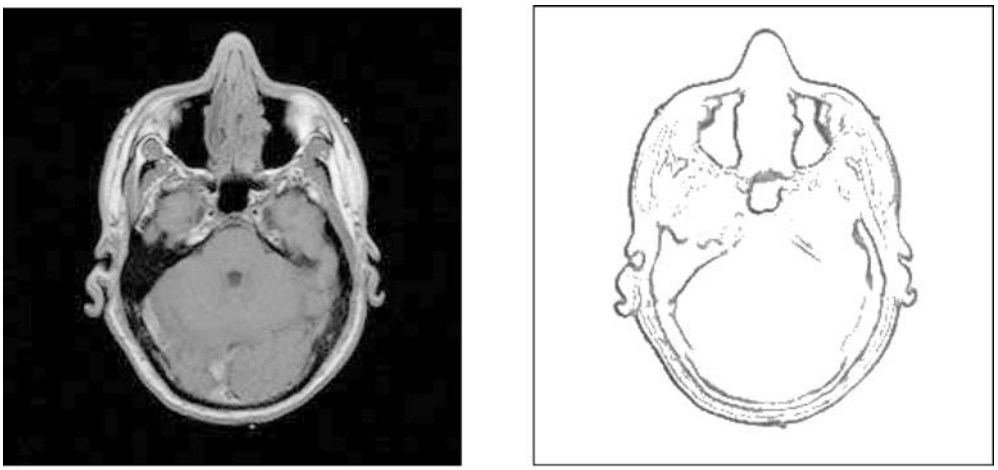

(a) (b)

Figure 3. An example of segmentation of a medical image. (a) Original image. (b) Result of segmentation. ($\mu = 0.1$, $\tau = 0.1$, $\sigma = 0.1$, $k = 0.1$, iteration $= 100$).

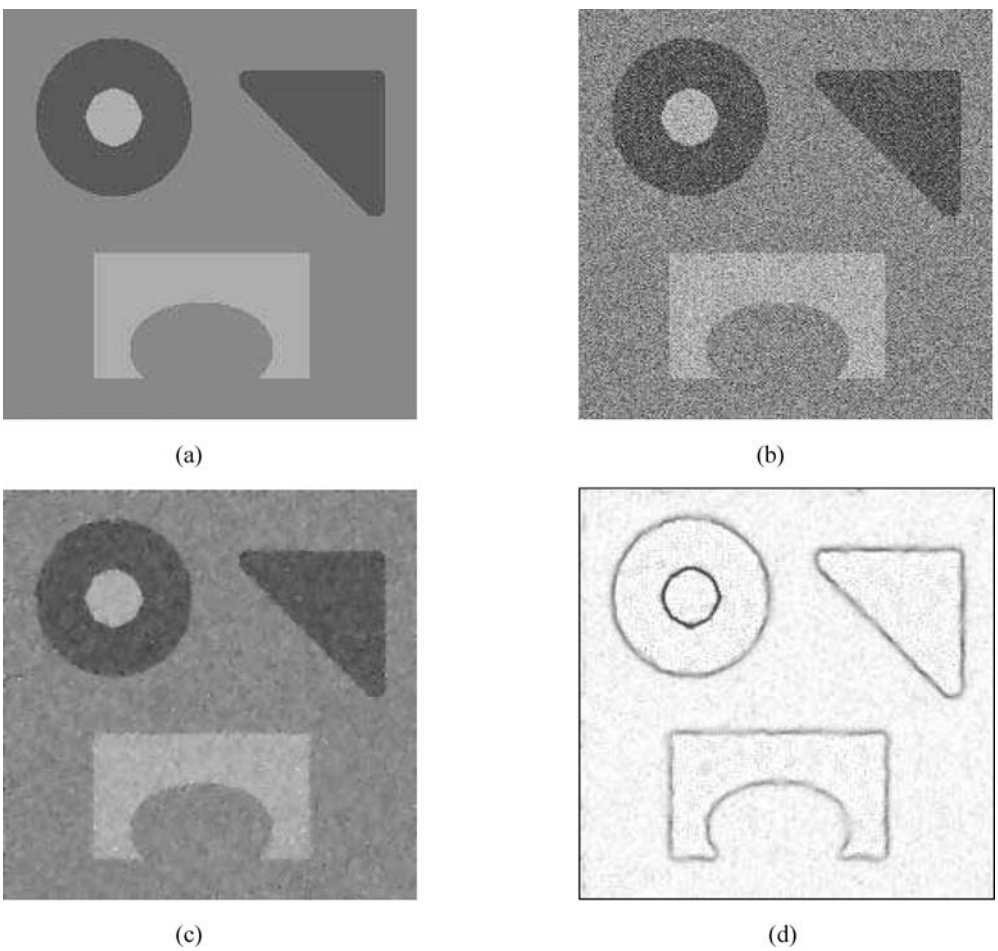

(a) (b)

(c) (d)

Figure 4. An example of image denoising and segmentation. (a) Original image. (b) Image with noise (SNR $= 8.4$). (c) Result of denoising. (d): Result of segmentation. ($\mu = 0.1$, $\tau = 0.1$, $\sigma = 1$, $k = 1$, iteration $= 70$).

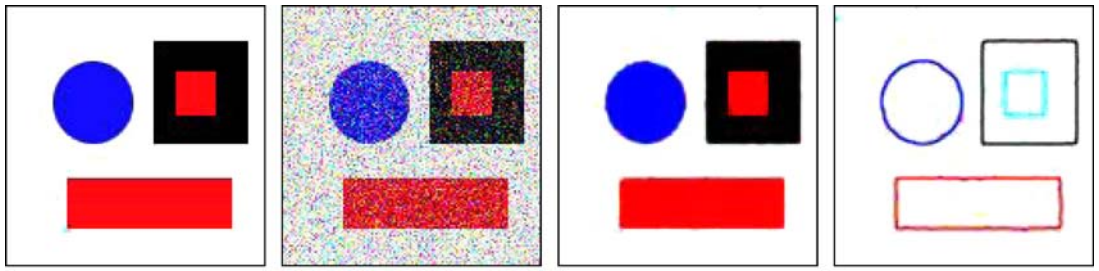

Figure 5. An example of color image denoising and segmentation (a) Original image. (b) Image with noise (SNR = 9.1). (c) Result of denoising. (d) Result of segmentation. ($\mu = 3, \tau = 0.1, \sigma = 1, k = 1$, iteration = 30).

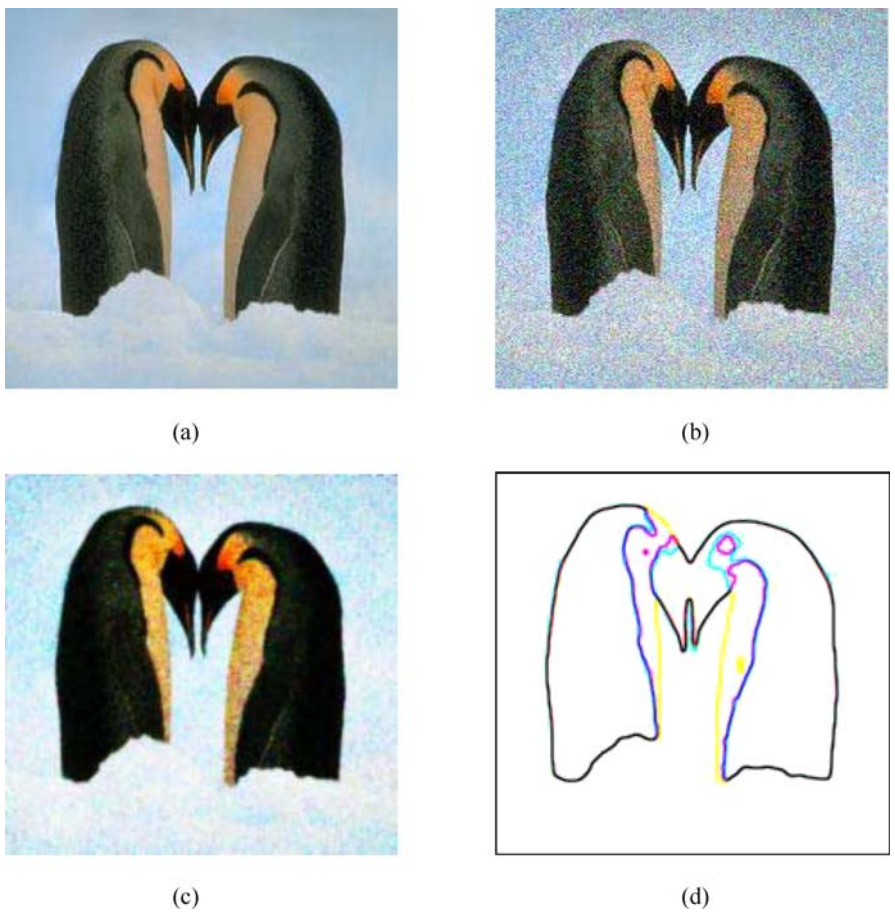

Figure 6. An example of color image denoising and segmentation (a) Original image. (b) Image with noise (SNR=15.2). (c) Result of denoising. (d) Result of segmentation. ($\mu = 3, \tau = 0.1, \sigma = 1, k = 10$, iteration = 10).

Theorem 4.1. *There exists a vector-valued function* $u_* : \Omega \to R^3$, $u_* \in g - BV(\Omega, R^3) \cap L^4(\Omega, R^3)$ *minimizing the energy* F_ε *in (11), where* ε *is a fixed positive constant.*

4.2. Numerical Implementation of the Model

The notations are the same as that in Section 3. The corresponding iterating scheme for (13) with respect

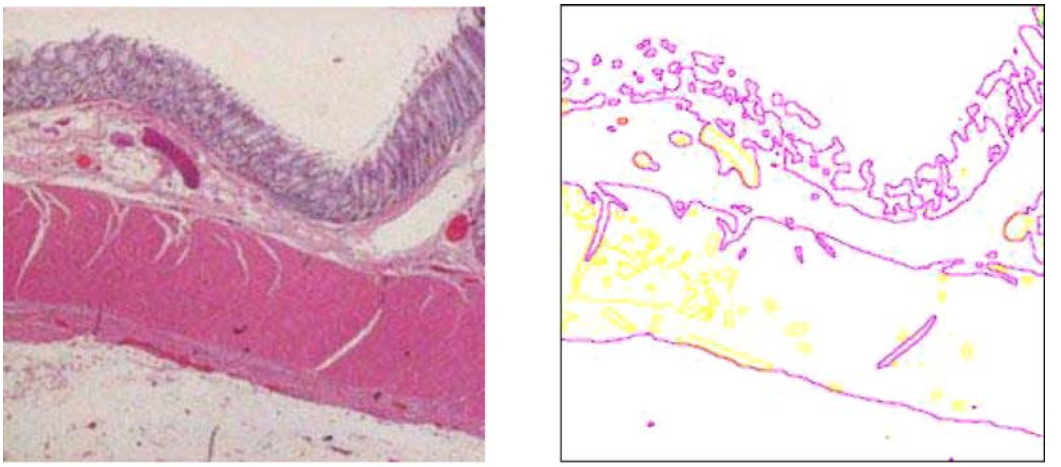

(a) (b)

Figure 7. An example of medical image segmentation. (a) Original image. (b) Result of segmentation. ($\mu = 1, \tau = 0.1, \sigma = 0.1, k = 10000$, iteration $= 100$).

(a) (b)

Figure 8. An example of natural image segmentation. (a) Original image. (b) Result of segmentation. ($\mu = 3, \tau = 0.1, \sigma = 0.1, k = 1$, iteration $= 60$).

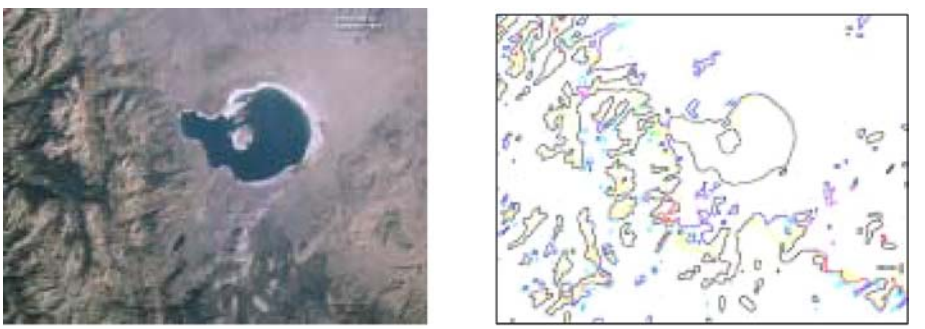

(a) (b)

Figure 9. An example of astronaut photography of Earth in Mono Lake, California, USA (STS047-94-32). Courtesy of the Image Science & Analysis Laboratory, NASA Johnson Space Center. (a) Original image. (b) Result of segmentation. ($\mu = 3, \tau = 0.1, \sigma = 0.1, k = 0.1$, iteration $= 100$).

to each component of u is:

$$u_1^{k+1} = u_1^k + \tau \cdot \left(A_1^k + \frac{1}{\varepsilon^2}\, u_1^k \left(1 - \left(u_1^k\right)^2\right) - \lambda \left(u_1^k - u_{01}\right) \right),$$

$$u_2^{k+1} = u_2^k + \tau \cdot \left(A_2^k + \frac{1}{\varepsilon^2}\, u_2^k \left(1 - \left(u_2^k\right)^2\right) - \lambda \left(u_2^k - u_{02}\right) \right),$$

$$u_3^{k+1} = u_3^k + \tau \cdot \left(A_3^k + \frac{1}{\varepsilon^2}\, u_3^k \left(1 - \left(u_3^k\right)^2\right) - \lambda \left(u_3^k - u_{03}\right) \right),$$

where

$$A_1^k = \mu \cdot \left(D_x^- \left(g \frac{D_x^+ u_1^k}{B^k} \right) + D_y^- \left(g \frac{D_y^+ u_1^k}{B^k} \right) \right),$$

$$A_2^k = \mu \cdot \left(D_x^- \left(g \frac{D_x^+ u_2^k}{B^k} \right) + D_y^- \left(g \frac{D_y^+ u_2^k}{B^k} \right) \right),$$

$$A_3^k = \mu \cdot \left(D_x^- \left(g \frac{D_x^+ u_3^k}{B^k} \right) + D_y^- \left(g \frac{D_y^+ u_3^k}{B^k} \right) \right),$$

$$B^k = \sqrt{\left|D\, u_1^k\right|^2 + \left|D\, u_2^k\right|^2 + \left|D\, u_3^k\right|^2 + \gamma},$$

and $\gamma > 0$ is a small number used to avoid division by zero.

4.3. Experimental Results

In our experiments for color images, we get $u = (u_1, u_2, u_3)$ after evolution. The segmented image is displayed by $255 \cdot \hat{u}$ where $\hat{u} = (u_1^2,\ u_2^2,\ u_3^2)$, and the denoised image is displayed by $(u + (1, 1, 1)) \cdot 255/2$. The reason for using $255 \cdot \hat{u}$ is as follows: by the second term in (11), after enough diffusion $|u_i| \approx 1$, $(i = 1, \ldots, 3)$ in the smoothed regions, and there exist at least one index $i \in \{1, 2, 3\}$ such that $|u_i|$ is near zero along edges. Therefore, $\hat{u} \approx (1, 1, 1)$ if and only if it is in the smoothed regions. Then $255 \cdot \hat{u}$ is displayed in white in the smoothed regions, and in other colors along edges. Hence, as a result of segmentation, the edges are displayed in color contours while the smoothed regions are in white, or more precisely, almost white. The reason for using $(u + (1, 1, 1)) \cdot 255/2$ as the denoised image is that $(u + (1, 1, 1)) \cdot 255/2$ is the rescaling of u, which is smoothed from the initial rescaled image u_0 by the evolution Eq. (13).

In Fig. 5, the original image is contaminated by gaussian noise with SNR = 9.1. Our model successfully denoises the image and gives the segmentation result. Compared with usual active contour methods, by which one must use two level sets to obtain the above segmentation result, our model is economical and efficient. In Fig. 6, gaussian noise with SNR=15.2 is added. The background color varies smoothly from sea to the cloudy sky. Our model smoothes the background, so after many times of diffusion, the background becomes almost white and the penguins are segmented. The phenomenon is due to the diffusion coefficient in (12), which is controlled by the gradient of f. In sharp edges, the gradient is very big, so the diffusion is very small. Hence, after many times of diffusion only sharp edges are still retained. More experimental results are given in Figs. 7 and 8. Our method successfully detects the edges of the medical image and the house image. In Fig. 9, an aerial image is segmented.

5. Conclusions

This paper describes a new method for image denoising and segmentation based on the GL model and the weighted BV model. When dealing with gray images, we use complex model which works better than the corresponding real model. However, for color images, we use vector-valued model directly without changing the observed image to image with more channels. Our numerical results confirm the effectiveness of our algorithm. Moreover, we have investigated the model mathematically and the existence of the minimizer to the energy functionals are proved. However, it remains to make a complete theoretical study of the associated flows for our energy functionals. This will be our future work.

Acknowledgments

This paper is partially supported by National Foundation of China (No. 10371039) and the Shanghai Priority Academic Discipline. We are grateful to anonymous referees for useful comments and suggestions.

References

1. G. Aubert, J.F. Aujol, and L.B. Feraud, "Detecting codimention-two objects in an image with Ginzburg-Landau models," to appear in *Int. J. Comput. Vis.*

2. G. Aubert and L. Vese, "A variational method in image recovery," *SIAM J. Numer. Anal.*, Vol. 34, No. 5, pp. 577–584 , 1997.
3. C.A.Z. Barcelos and Y. Chen, "Heat flows and related minimization problem in image restoration," *Comput. Mat. App.*, Vol. 39, pp. 81–97, 2000.
4. F. Bethuel, H. Brezis, and F. Helein, "Singular limit for the minimization of Ginzburg-Landau functionals," *CRAS I-MATH*, Vol. 314, pp. 891–895, 1992.
5. P.V. Blomgren and T.F. Chan, "Color TV: Total variation methods for restoration of vector valued images," *IEEE Trans. Image Process.*, Vol. 7, pp. 304–309, 1998.
6. V. Caselles, R. Kimmel, and G.. Sapiro, "Geodesic active contours," *Int. J. Comput. Vis.,* Vol. 22, No. 1, pp. 61–79, 1997.
7. T.F. Chan, S.H. Kang, and J. Shen, "Total variation denoising and enhancement of color images based on the CB and HSV color models," *J. Vis. Commun. Image Rep.,* Vol. 12, pp. 422–435, 2001.
8. T.F. Chan, S. Osher, and J. Shen, "The digital TV filter and nonlinear denoising," *IEEE Trans. Image Process.,* Vol. 10, No. 2, pp. 231–241, 2001.
9. T.F. Chan and J. Shen, "Variational restoration of non-flat image features: Models and algorithms," *SIAM J. App. Math.*, Vol. 61, pp.1338–1361, 2000.
10. T.F. Chan and L.A. Vese, "Active contour without edges," *IEEE Trans. Image Process.*, Vol. 22, pp. 61–79, 1997.
11. X.Y. Chen, S. Jimbo, and Y. Morita, "Stablization of vortices in the Ginzburg-Landau equation with variable diffusion coefficients," *SIAM J. Math. Anal.*, 1998.
12. Y. Chen and T. Wunderli, "Adaptive total variation for image restoration in BV space," *J. Math. Anal. Appl.,* Vol. 272, pp. 117–137, 2002.
13. M. Kass, A. Witkin, and D. Terzopoulos, "Snakes: Active contour models," *Int. J. Comput. Vis.,* Vol. 1, pp. 321–331, 1988.
14. F.H. Lin and X.P. Yang, *Geometric Measure Theory-An Introduction*, *Advanced Mathematics*. International Press: Boston, 2001.
15. S. Osher, A. Sole, and L. Vese, "Image decomposition and restoration using total variation minimization and the H^{-1} norm," *SIAM J. Multiscale Model. Simu.,* Vol. 1:3, pp. 349–370, 2003.
16. L. Rudin, S. Osher, and E. Fatemi, "Nonlinear total variation based noise removal algorithms," Physica D., Vol. 60, pp. 259–268, 1992.
17. B. Tang, G. Sapiro, and V. Caselles, "Diffusion of general data on non-flat manifolds via Harmonic maps theory: The direction diffusion case,"*Int. J. Comput. Vis.*, Vol. 36, pp. 149–161, 2000.
18. B. Tang, G. Sapiro, and V. Caselles, "Color image enhancement via chromaticity diffusion," *IEEE Trans. Image Process.,* Vol. 10, pp. 701–707, 2001.
19. P.E. Trahanias, D. Karako, and A.N. Venetsanopoulos, "Directional processing of color images: Theory and experimental results," *IEEE Trans. Image Process.*, Vol. 5, No. 6, pp. 868–880, 1996.
20. L. Vese and S. Osher, "Modeling textures with total variation minimization and oscillating patterns in image processing," *J. Sci. Comput.*, Vol. 19, No. 1–3, pp. 553–572, 2003.

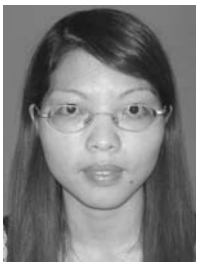

Fang Li received the MSc degree in Mathematics from the South West China Normal University in 2004 and from then on she works in the South West University. Meanwhile, she studies mathematics at the East China Normal University as a doctoral student. Her research interests include anisotropic diffusion filtering, the variational methods and PDEs in image processing.

Chaomin Shen received the MSc degree in Mathematics from the National University of Singapore (NUS) in 1998. He worked in the Centre for Remote Imaging, Sensing and Processing (CRISP), NUS as an associate scientist during 1998 to 2004. Currently he is a lecturer in Joint Laboratory for Imaging Science & Technology and Department of Computer Science, East China Normal University. His research interests include remote sensing applications and variational methods in image processing.

Ling Pi received her MSc degree from the Department of Mathematics, East China Normal University in 2003. She is currently a lecturer in the Department of Applied Mathematics, Shanghai Jiaotong University. Her work involves the application of geometric and analytic methods to problems in image processing.